ЖЭТФ, 2016, том 149, вып. 6, стр. 1157–1163

TWO STRONGLY CONTRASTING Λ-SYSTEMS IN THE D_1 LINE OF ^{87}Rb IN A TRANSVERSE MAGNETIC FIELD

A. Sargsyan [a], *D. Sarkisyan* [a*], *L. Margalit* [b], *A. D. Wilson-Gordon* [b]

[a] *Institute for Physical Research, National Academy of Sciences of Armenia*
0203, Ashtarak, Armenia

[b] *Department of Chemistry, Bar-Ilan University*
5290002, Ramat Gan, Israel

Received January 19, 2016

Four different types of spectroscopic cells that cover all possible existing versions of sealed-off cells (containing alkali atomic vapor) characterized by drastically different relaxation rates γ_{rel} are used to study the electromagnetically-induced-transparency spectra of two Λ-systems in the D_1 line of ^{87}Rb in the presence of a transverse magnetic field. Two cw narrowband diode-lasers are used to form the coupling laser radiation (with a fixed frequency) and the probe radiation with a tunable frequency. Two strongly contrasting Λ-systems are found: the first shows resonances that are transformed from dark resonances to bright resonances in all cases apart from nanocells, whereas the second shows four dark resonances in all four different types of cell. The theoretical simulations are in good agreement with the experimental results.

DOI: 10.7868/S0044451016060067

1. INTRODUCTION

The electromagnetically induced transparency (EIT) phenomenon in alkali metal vapor in an external magnetic field was extensively studied from the 1990s onwards [1–4]. We also note the seminal paper by Bell and Bloom [5], published much earlier. In particular, ultra-narrow (optical domain) EIT resonances were used to measure weak magnetic fields of 1 mG. Recent investigations of the EIT resonances in strong magnetic fields [6–10] are interesting from a purely scientific standpoint as well as for applications, because they allow forming tunable narrow optical reference resonances that are displaced by several gigahertz from the unperturbed atomic transitions [11]. These can be used in laser frequency stabilization, which is often needed in practice [12], and also for the formation of strongly displaced frequency references with a spectral resolution of a few megahertz, which is much more accurate than available instruments.

In addition, the study of N-type resonances (which have similar parameters to the EIT resonances) in strong magnetic fields is also important for scientific and practical reasons [13, 14]. We note that the same ground levels of the alkali metals are involved in both EIT and N-type resonance splitting in magnetic fields.

The study of EIT in a transverse magnetic field (TMF) is of a special interest because additional accompanying processes can occur [15–17]. Recently, it was demonstrated experimentally that the study of EIT in TMFs can give additional important information, particularly, evidence of the influence of the alignment process [17]. The alignment process [18, 19] causes the sign reversal from a dark resonance (DR) to a bright resonance (BR) which we call a "resonance inverted by alignment (RIA)". It was established in [17] that the most convenient Λ-system for RIA observation is the one shown in Fig. 1*a*, where ν_C is in resonance with the $1 \to 1'$ transition, while ν_P is scanned through the $2 \to 1'$ transition (the configuration of the laser electric fields and the TMF is shown in Fig. 1*c*). The alignment process is very effective due to strong Zeeman optical pumping. Because the alignment process strongly depends on the decay rate γ_{rel} of the coherence between the lower levels, it was demonstrated that the EIT features strongly depend on the type of cell used for the atomic vapor [17].

The aim of this paper is to show the existence of a unique Λ-system in the D_1 line of ^{87}Rb (see Fig. 1*b*) where all four resonances remain dark in the presence of a TMF, although they are formed in four different

* E-mail: davsark@yahoo.com

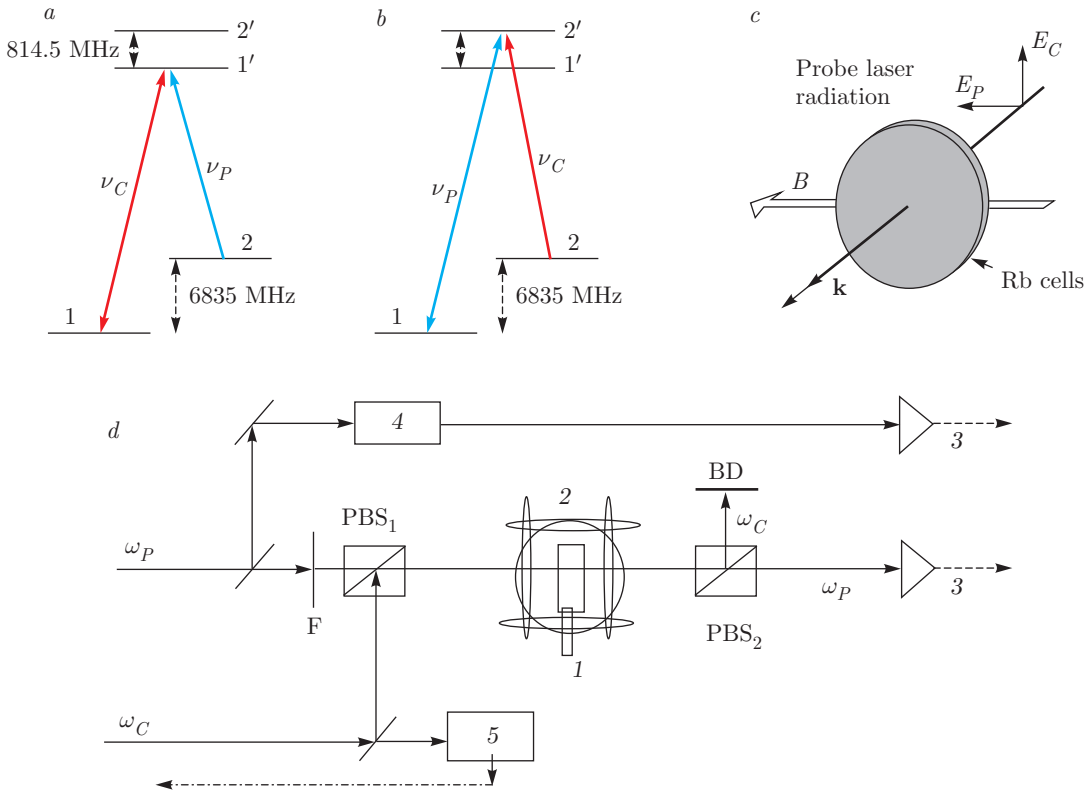

Fig. 1. (*a*) and (*b*) Two Λ-systems that are studied, (*c*) the configuration of the magnetic field **B** and the electric fields $\mathbf{E}_C$, $\mathbf{E}_P$ and the direction **k** of the laser radiation propagation. (*d*) Experimental setup. Two cw narrowband (1 MHz) diode-lasers are used. The coupling with a fixed frequency ω_c and the probe with a tunable frequency ω_P: PBS$_{1,2}$ — polarizing beam splitters; *1* — four sealed-off cell filled with Rb; *2* — Helmholtz coils; *3* — photodetectors; *4* — reference nanocell; *5* — the unit for the "error" signal formation and stabilization of the laser frequency ν_C; F — filters; BD — beam damper

types of vapor cells that have drastically different relaxation rates γ_{rel}.

2. EXPERIMENT

2.1. Four different type cells

Four different types of sealed-off cells filled with Rb atomic vapor are used: 1) a 1-cm-long T-shaped cell of the usual type (that is, with a side-arm), which is 15 mm in diameter and has sapphire windows 0.5 mm in thickness (with the *c*-axis perpendicular to the surface to avoid birefringence); 2) an 8-mm-long glass or sapphire cell with an antirelaxaition coating of PDMS [20]; 3) a 0.5-mm-thick sapphire cell with neon buffer gas at a pressure of 23 Torr [13]; 4) a nanometric thin cell nanocell of the thickness $L = \lambda = 795$ nm (more details on the cell design can be found in [21]). We note that these four types of cells cover all possible versions of sealed-off cells (containing alkali atomic vapor) available at the present time.

2.2. Experimental setup

The experimental arrangement is sketched in Fig. 1*d*. The beams of two separate single-frequency extended-cavity diode lasers with $\lambda \approx 795$ nm and 1 MHz linewidth are used (not shown in the figure). One of the lasers (coupling laser) operates at a fixed frequency ν_C, while the frequency ν_P of the other laser (probe laser) is tunable. Both laser beams with a diameter of 1.3 mm overlap in the polarizing beam splitter PBS$_1$ (the coupling and probe lasers have orthogonal linear polarizations) and are incident on each of the four different types of cells. To prevent optical feedback, Faraday isolators have been used (not shown in the figure). Each cell *1* is placed in turn inside the three pairs of mutually perpendicular Helmholtz coils *2* that allow us to cancel the laboratory magnetic field as well as to apply a homogeneous transverse magnetic field. An external magnetic field **B** is directed along the probe field $\mathbf{E}_P$, while $\mathbf{E}_C$ is perpendicular to the **B** field (see Fig. 1*c*). Part of the probe radiation was

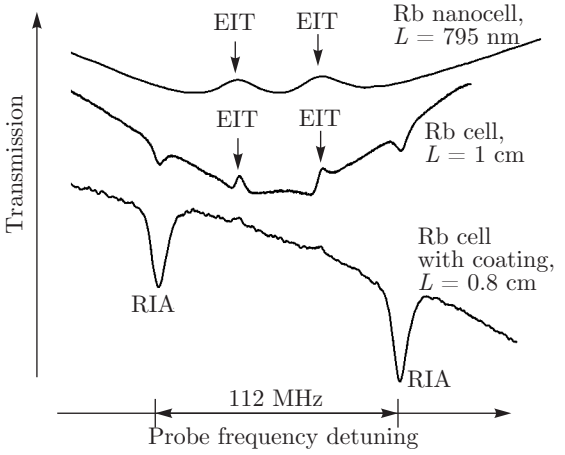

Fig. 2. D_1 line of ^{87}Rb. The EIT spectra for the Rb nanocell with thickness $L = \lambda = 795$ nm, $T = 110\,^{\circ}$C (upper curve): two DRs are shown. The middle spectrum for the Rb 1-cm-long cell, two DRs, and two RIAs with nearly the same amplitudes are shown, $T = 36\,^{\circ}$C (a similar spectrum can be obtained with the use of a Rb 0.5-mm-thin cell filled with neon gas). For the antirelaxation-coating cell, $T = 36\,^{\circ}$C (lower curve), two small DRs and two large RIA are shown. The probe power is $P_P = 0.2$ mW, coupling power is 13.6 mW, and $B \approx 27$ G

sent into a reference nanocell *4* of the thickness $L = \lambda$ to form a frequency reference. As was shown in [7], narrow velocity selective optical pumping resonances, which are located at the atomic transitions, appear in the transmission spectrum and serve as the atomic transition markers. The beams were detected using FD-24K photodiodes *3*. The photodiode signals were amplified in an operational amplifier and were displayed on a Tektronix TDS2014B four-channel digital oscilloscope. A fraction of laser radiation ν_C was guided to system *5* for the formation of an "error" signal and the stabilization of the laser frequency ν_C [22].

2.3. Experimental results

To understand the results obtained for the Λ-system shown in Fig. 1*b*, we first present the results (Fig. 2) obtained for the Λ-system shown in Fig. 1*a* using three different types of cells filled with Rb vapor. The upper spectrum is for the nanocell thickness $L = \lambda = 795$ nm and consists of the usual EIT resonances, demonstrating a reduction in the absorption. The middle spectrum is for the 1-cm-long cell; here, there are two DRs and two RIAs with nearly the same amplitudes. We note that a similar spectrum can be obtained with the use of an Rb 0.5-mm-thin cell filled with neon gas (not shown in the figure). The lower spectrum is for the case of an 8-mm-long antirelaxation-coating cell. Here, there are two large RIAs and two small DRs, which vanish when the probe power is > 0.3 mW [7]. The respective coupling and probe laser powers are 13.6 mW and 0.2 mW, and the magnetic field is $B \approx 27$ G. We note that the results obtained with these two additional cells characterized by a moderate value of γ_{rel} complement the results already published.

Thus, we conclude that RIA is always present for the Λ-system in Fig. 1*a*. A detailed explanation of this unusual behavior is presented in [17]. Briefly, due to Zeeman optical pumping caused by the π-polarization of the strong probe, the population of the level $F_g = 2$ is trapped in the sublevels with $m_F = \pm 2$, that is, alignment occurs [18, 19]. Thus, the alignment causes a strong redistribution of the population of the $F_g = 2$ level. The increase (or reduction) in the population N of the $m_F = \pm 2$ Zeeman sublevels with $F_g = 2$ is [18, 19]

$$\Delta N \sim \frac{(dE_P/\hbar)^2}{\gamma_N \gamma_{rel}},$$

where $(dE_P/\hbar)$ is the Rabi frequency of the probe laser and γ_N is the natural linewidth. We thus see that ΔN strongly depends on the relaxation rate γ_{rel}. For a 1-cm-long cell, it is inversely proportional to the time of flight of the atom across the laser beam with a diameter D. For D about 1 mm, γ_{rel} is typically about 100 kHz. For the antirelaxation-coating cell, it is about 1 kHz due to the not high quality of coating, while an advantage of this coated cell is its resistance to temperatures up to 150 °C [20]. For the nanocell, the relaxation rate is much higher ($\gamma_{rel} > 1$ MHz). This is related to frequent collisions of the Rb atoms with the nanocell windows, destroying the alignment process. Hence, for the Λ-system presented in Fig. 1*a*, all three types of cells (apart from the nanocell) demonstrate formation of RIAs. For other possible laser frequency configurations, the alignment is weaker [17] due to the additional redistribution of the population between the Zeeman sublevels caused by the strong coupling laser.

We now present the results obtained with the use of Λ-system shown in Fig. 1*b* and compare them with the above results. The transmission spectra of a 1-cm-long Rb cell are shown in Fig. 3. The upper curve shows the EIT resonance for zero magnetic field. The middle curve shows four DRs when a TMF $B \approx 25$ G is applied. The linewidth of the DRs is 5 MHz (FWHM). The lower curve is the reference and shows the transition 1–2′.

The diagram presented in Fig. 4 clarifies the origin of the four DRs and the frequency intervals between

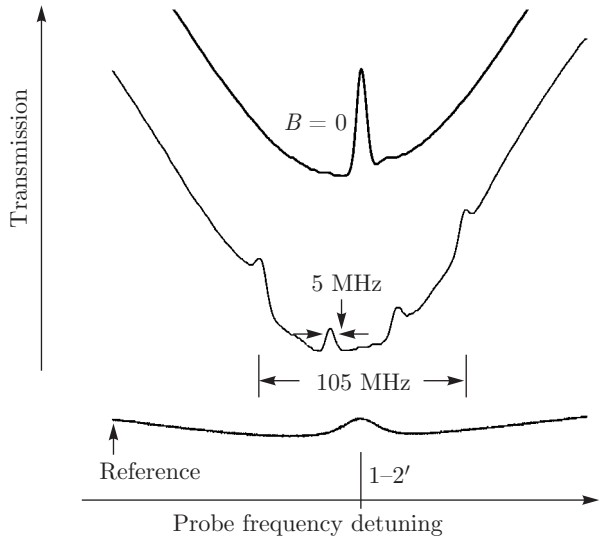

Fig. 3. Transmission spectra of a 1-cm-long Rb cell. The upper spectrum shows DR for $B = 0$, $P_C = 10$ mW, and $P_P = 0.3$ mW. The middle spectrum shows four DRs at $B \approx 25$ G. The linewidth of the DRs is 5 MHz, the lower curve is the reference spectrum

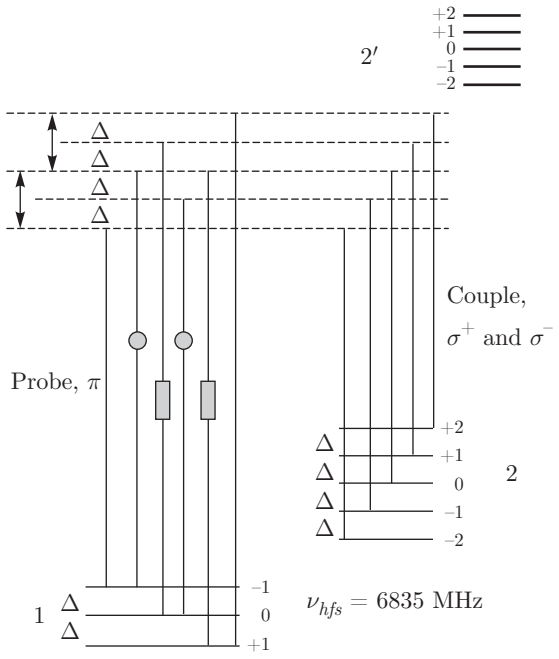

Fig. 4. D_1 line of ^{87}Rb, the EIT process. The coupling laser has the fixed frequency ν_C and σ^+ and σ^- polarizations, while the probe laser has π-polarization and the frequency ν_P is varied. Degenerate frequencies are indicated by circles and rectangles. There are four different DR frequencies. The frequency interval between the neighboring DRs is $2 \cdot 0.7$ MHz/G $= 1.4$ MHz/G

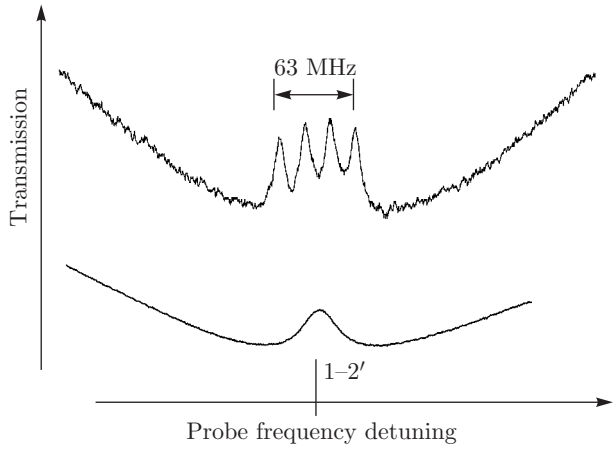

Fig. 5. Transmission spectra of a 0.8-cm-long antirelaxation-coating cell, the upper spectrum shows four DRs (the linewidth ~ 7 MHz) for $B = 15$ G, $P_C = 13$ mW, and $P_P = 0.5$ mW, the lower curve is the reference spectrum

the neighboring DRs. The coupling laser has a fixed frequency ν_C and σ^+ and σ^- polarizations, while the probe laser has π-polarization and the frequency ν_P is varied. The selection rules are $\Delta m_F = 0$ for the atomic transitions in the case of π-polarizations between the Zeeman sublevels of the ground and excited levels, and $\Delta m_F = \pm 1$ for the respective σ^+ and σ^- polarizations. As we see, there are six Λ-systems formed. However, there are two pairs that contain two degenerate frequencies. For the first pair, they are indicated by circles and for the second pair, the degenerate frequencies are indicated by rectangles. Hence, there are four different DR frequencies. The frequency interval between the neighboring DRs is $2 \cdot 0.7$ MHz/G $= 1.4$ MHz/G. This value is correct for $B \leq 50$ G. We note that in [7], results for EIT in a magnetic field are presented for the ^{87}Rb D_1 line for the ν_C and ν_P configuration shown in Fig. 1*b*, and four EIT resonances are also reported, as shown in Figs. 3–5. However, the diagram shown in Fig. 1 in [7] is incorrect, because the coupling laser frequency varies, rather than being constant as shown in Fig. 4.

The transmission spectra of a 0.8-cm-long antirelaxation-coating cell are shown in Fig. 5. The upper curve shows four DRs when the TMF $B = 15$ G is applied. The lower curve is the reference and shows the position of the velocity selected optical pumping that is located at the transition 1–2′. In Fig. 6, the transmission spectra of a 0.5-mm-thick cell with neon buffer gas are presented. The upper curve shows the EIT resonance for a zero magnetic field. The next spectrum shows four DRs for $B = 25$ G. The third spectrum from

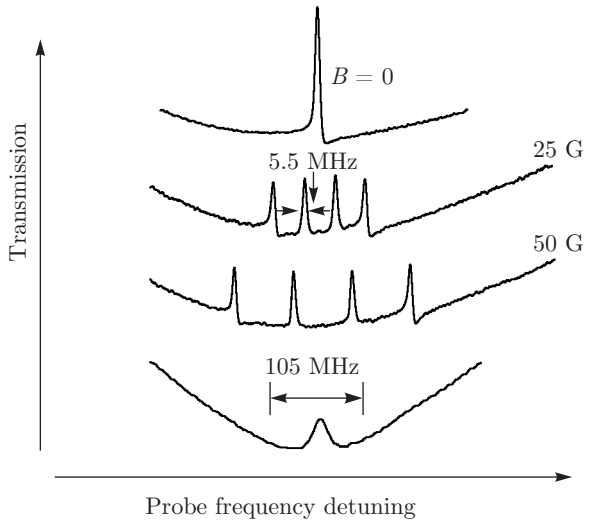

Fig. 6. Transmission spectra of a 0.5-mm-thick cell filled with neon; the upper curve shows DR for $B = 0$, the second and the third from top are four DRs at $B = 25$ G and $B = 50$ G, respectively, $P_C = 10$ mW, and $P_P = 0.3$ mW. The linewidth of the DR is 5.5 MHz, the lower curve is the reference

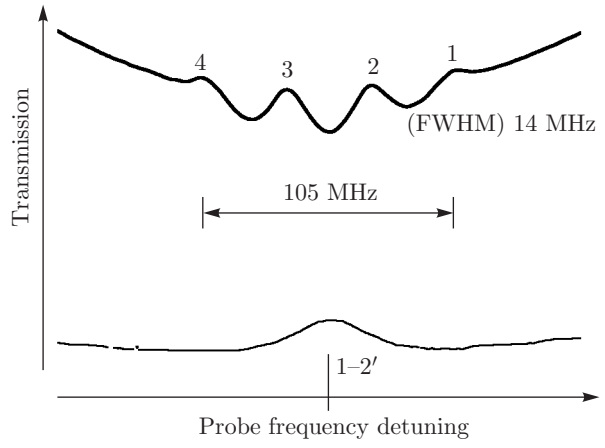

Fig. 7. Rb nanocell, $L = 795$ nm, $B = 25$ G, the upper spectrum shows four DRs at $B = 26$ G, $P_C = 13$ mW, and $P_P = 0.5$ mW, the linewidth of the DR components is 14 MHz (FWHM), and the lower curve is the reference

top shows four DRs for $B = 50$ G. The lower curve is the reference and shows the position of the transition 1–$2'$.

The upper curve in Fig. 7 shows the transmission spectra of the nanocell with the thickness $L = \lambda = 795$ nm. Four DRs occur when $B = 25$ G. The lower curve is the reference and shows the position of the transition 1–$2'$. Thus, for the Λ-system presented in Fig. 1*b*, all four types of cell demonstrate the formation of four DRs. This means that the influence of the alignment process is negligible for this Λ-system.

We note that the values of the coupling and the probe powers used for the results presented in Figs. 5 and 7 are the same, and hence the additional broadening of the linewidth in the case of the nanocell is caused by the larger value of γ_{rel} due to frequent atom–wall collisions.

3. THEORETICAL MODEL

The theoretical model that has been used to calculate the probe transmission spectra is described in detail in Refs. [16, 23]. This realistic model includes all the sublevels that comprise the full atomic system and all the relaxation processes that occur but does not take Doppler broadening into account. We solved the steady-state Bloch equations for the Λ-system shown in Fig. 1*b* for the three types of Rb cells, where the ground hyperfine levels are $F_g = 2$, $F_{g'} = 1$ and the excited hyperfine level is $F_e = 2$. The decay rates of the coherence between the Zeeman sublevels e_i of the excited state F_e and the Zeeman sublevels g_j of the ground state F_g are given by

$$\Gamma'_{e_i g_j} = \gamma + \\ + \frac{1}{2}\left[\Gamma + (2F_g)\Gamma_{g_i g_j} + (2F_{g'}+1)\Gamma_{g_i g'_j}\right] + \Gamma^*, \quad (1)$$

where γ is the rate of decay due to the time of flight through the laser beams, $\Gamma_{g_i g_j}$ and $\Gamma_{g_i g'_j}$ are the collisional decay rates of the F_g sublevels to other F_g and $F_{g'}$ sublevels, and Γ^* is the rate of phase-changing collisions from the excited states to the ground state. An expression similar to Eq. (1) can be written for $\Gamma'_{e_i g'_j}$. To simulate the effect of Doppler broadening, we use Γ^* as a fitting parameter since both Doppler broadening and phase-changing collisions lead to a narrowing of the DR linewidth [24]. The theoretical results are shown in Fig. 8 for a pure Rb cell, an Rb antirelaxation-coating cell and an Rb cell with neon. The experimental coupling laser powers were converted to Rabi frequencies in accordance with [25]. It should be noted that the inner pair of DRs are broader than the outer DRs due to the greater values of the $3j$ symbols and consequently the effective Rabi frequency. The behavior of the EIT resonance shapes, widths, and frequencies are in good agreement with the experimental data. In connection with the nanocell, we note that further improvement in the model is necessary to properly describe the EIT for the nanocell.

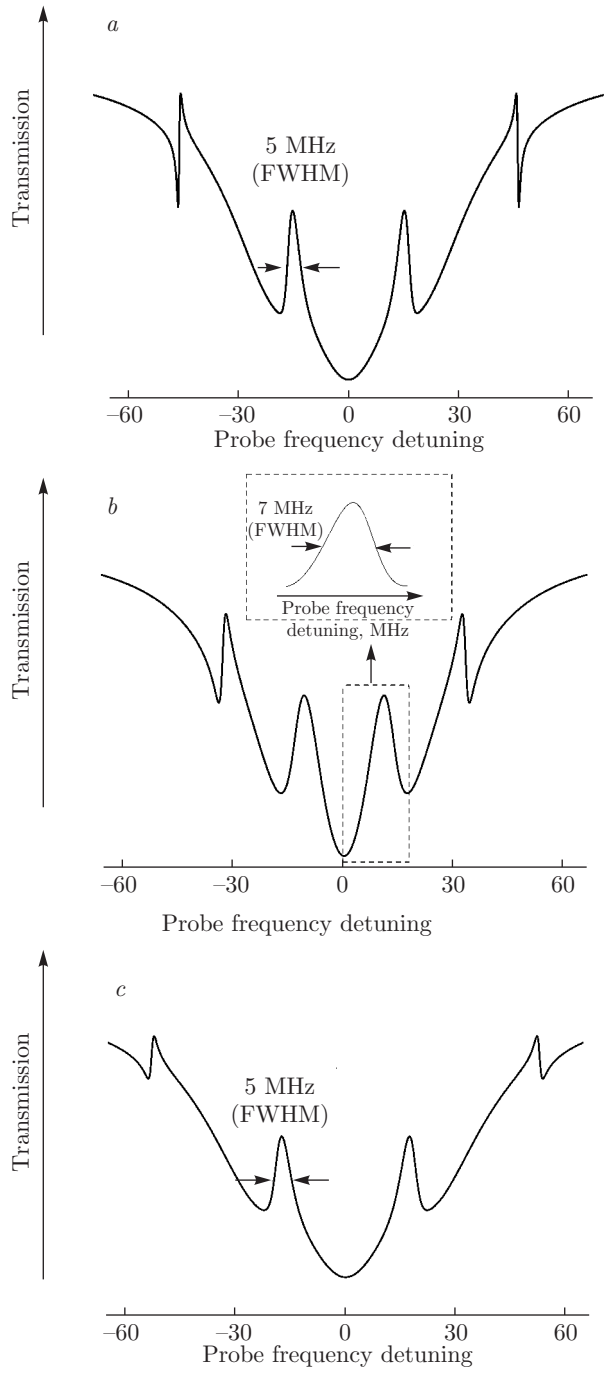

Fig. 8. Theoretical transmission spectra for the three types of Rb cells. (a) A pure Rb cell. The parameters used in the calculation are $\Omega_C = 52$ MHz, $B = 25$ G, $\Gamma^* = 17$ MHz, $\gamma = 0.1$ MHz, and $\Gamma_{g_i g_j} = \Gamma_{g_i g'_j} = 0$; ($b$) an Rb antirelaxation-coating cell, $B = 15$ G, $\Omega_C = 64$ MHz, $\Gamma^* = 17$ MHz, $\gamma = 1$ kHz, and $\Gamma_{g_i g_j} = \Gamma_{g_i g'_j} = 0$; ($c$) an Rb cell with neon, $B = 25$ G, $\Omega_C = 52$ MHz, $\Gamma = 17$ MHz, $\gamma = 0.1$ MHz, and $\Gamma_{g_i g_j} = 0$, $\Gamma_{g_i g'_j} = 0.2$ MHz. The linewidths of DRs (5, 7, and 5.5 MHz) have been measured after subtracting the slopes, as is shown in the inset to Fig. 8b

4. CONCLUSION

Two selected Λ-systems in the D_1 line ^{87}Rb are used to demonstrate drastically different behavior of the EIT resonances in a TMF. For this purpose, four different types of spectroscopic cells that cover all possible existing versions of sealed-off cells and provide strongly varying values of the relaxation rate γ_{rel} have been used. For the first Λ-system, the coupling frequency is in resonance with the $1 \to 1'$ transition, while the probe is scanned through the $2 \to 1'$ transition. In all the cells apart from the nanocell, this allows the formation of resonances, which are transformed from dark to bright. In this case, the influence of the alignment process is crucial to justify the term RIA (resonance inverted by alignment). For the second Λ-system, the coupling frequency is in resonance with the $2 \to 2'$ transition, while the probe is scanned through the 1–$2'$ transition. This allows the formation of four DRs in all four types of the Rb cells. For this Λ-system, the influence of the alignment process is negligible.

This paper was supported by a Marie Curie International Research Staff Exchange Scheme Fellowship within the 7th European Community Framework Program "Coherent optics sensors for medical applications-COSMA" (grant agreement No. PIRSES-GA-2012-295264). A. S. and D. S. gratefully acknowledge the financial support of the State Committee for Science of the Ministry of Education and Science of the Republic of Armenia in the framework of project No. 15T-1C040.

REFERENCES

1. A. M. Akulshin, A. A. Celikov, and V. L. Velichansky, Opt. Comm. **84**, 139 (1991).

2. R. Wynands, A. Nagel, S. Brandt et al., Phys. Rev. A **58**, 196 (1998).

3. R. Wynands and A. Nagel, Appl. Phys. B **68**, 1 (1999).

4. M. Fleischhauer, A. Imamoglu, and J. P. Marangos, Rev. Mod. Phys. **77**, 633 (2005).

5. W. E. Bell and A. L. Bloom, Phys. Rev. Lett. **6**, 280 (1961).

6. K. Motomura and M. Mitsunaga, J. Opt. Soc. Amer. B **19**, 2456 (2002).

7. X. Wei, J. Wu, G. Sun et al., Phys Rev. A **72**, 023806 (2005).

8. A. Sargsyan, R. Mirzoyan, T. Vartanyan, and D. Sarkisyan, Zh. Eksp. Teor. Fiz. **145**, 414 (2014).

9. N. Gavra, M. Rosenbluh, T. Zigdon et al., Opt. Comm. **280**, 374 (2007).

10. A. Sargsyan, R. Mirzoyan, and D. Sarkisyan, Pis'ma v Zh. Eksp. Teor. Fiz. **96**, 333 (2012).

11. D. Sarkisyan, A. Sargsyan, J. Keaveney, and C. S. Adams, Zh. Eksp. Teor. Fiz. **146**, 13 (2014).

12. A. Sargsyan, A. Tonoyan, R. Mirzoyan et al., Opt. Lett. **39**, 2270 (2014).

13. A. Sargsyan, R. Mirzoyan, A. Papoyan, and D. Sarkisyan, Opt. Lett. **37**, 4871 (2012).

14. D. Slavov, A. Sargsyan, D. Sarkisyan et al., J. Phys. B **47**, 035001 (2014).

15. L. Margalit, M. Rosenbluh, and A. D. Wilson-Gordon, Phys. Rev. A **87**, 033808 (2013).

16. L. Margalit, M. Rosenbluh, and A. D. Wilson-Gordon, Phys. Rev. A **88**, 023827 (2013).

17. A. Sargsyan, D. Sarkisyan, Y. Pashayan-Leroy et al., Zh. Eksp. Teor. Fiz. **148**, 1104 (2015).

18. M. Auzinsh, D. Budker, and S. M. Rochester, *Optically Polarized Atoms*: *Understanding Light–Atom Interactions*, Oxford Univ. Press (2010).

19. D. Budker, D. F. Kimball, and D. P. DeMille, *Atomic Physics*, Oxford Univ. Press (2004).

20. S. Gozzini and A. Lucchesini, Eur. Phys. J. D **28**, 157 (2004).

21. A. Sargsyan, G. Hakhumyan, R. Mirzoyan, and D. Sarkisyan, Pis'ma v Zh. Eksp. Teor. Fiz. **98**, 499 (2013).

22. A. Sargsyan, A. V. Papoyan, D. Sarkisyan, and A. Weis, Eur. Phys. J. Appl. Phys. **48**, 20701 (2009).

23. L. Margalit, M. Rosenbluh, and A. D. Wilson-Gordon, Phys. Rev. A **85**, 063809 (2012).

24. A. Javan, O. Kocharovskaya, H. Lee, and M. O. Scully, Phys. Rev. A **66**, 013805 (2002).

25. B. E. King, arXiv:0804.4528 [physics.atom-ph].